applied sciences

MDPI

Article

# Integrated Field Surveying and Land Surface Quantitative Analysis to Assess Landslide Proneness in the Conero Promontory Rocky Coast (Italy)

**Francesco Troiani [1], Salvatore Martino [1], Gian Marco Marmoni [1], Marco Menichetti [2], Davide Torre [1], Giulia Iacobucci [1] and Daniela Piacentini [2,*]**

[1] Department of Earth Sciences, Sapienza University of Rome, 00185 Rome, Italy; francesco.troiani@uniroma1.it (F.T.); salvatore.martino@uniroma1.it (S.M.); gianmarco.marmoni@uniroma1.it (G.M.M.); davide.torre1993@gmail.com (D.T.); giulia.iacobucci@uniroma1.it (G.I.)

[2] Department of Pure and Applied Sciences, University of Urbino "Carlo Bo", 61029 Urbino PU, Italy; marco.menichetti@uniurb.it

* Correspondence: daniela.piacentini@uniurb.it

Received: 16 June 2020; Accepted: 8 July 2020; Published: 13 July 2020


**Featured Application: Assessment of landslide proneness, with a particular emphasis on catastrophic landslide events.**

**Abstract:** Rock slopes involved in extensive landslide processes are often characterized by complex morphodynamics acting at different scales of space and time, responsible for different evolutionary scenarios. Mass Rock Creep (MRC) is a critical process for long-term geomorphological evolution of slopes and can likewise characterize actively retreating coastal cliffs where, in addition, landslides of different typologies and size superimpose in space and time to marine processes. The rocky coast at the Conero promontory (central Adriatic Sea, Italy) offers a rare opportunity for better understanding the predisposing role of the morphostructural setting on coastal slope instability on a long-time scale. In fact, the area presents several landslides of different typologies and size and state of activity, together with a wide set of landforms and structural features effective for better comprehending the evolution mechanisms of slope instability processes. Different investigation methods were implemented; in particular, traditional geomorphological and structural field surveys were combined with land surface quantitative analysis based on a Digital Elevation Model (DEM) with ground-resolution of 2 m. The results obtained demonstrate that MRC involves the entire coastal slope, which can be zoned in two distinct sectors as a function of a different morphostructural setting responsible for highly differentiated landslide processes. Therefore, at the long-time scale, two different morphodynamic styles can be depicted along the coastal slopes that correspond to specific evolutionary scenarios. The first scenario is characterized by MRC-driven, time-dependent slope processes involving the entire slope, whereas the second one includes force-driven slope processes acting at smaller space–time scales. The Conero promontory case study highlights that the relationships between slope shape and structural setting of the deforming areas are crucial for reaching critical volumes to induce generalized slope collapse as the final stage of the MRC process. The results from this study stress the importance of understanding the role of morphostructures as predisposing conditions for generalized slope failures along rocky coasts involved in MRC. The findings discussed here suggest the importance of the assessment of the slope instability at the long time scale for a better comprehension of the present-day slope dynamics and its major implications for landslide monitoring strategies and the hazard mitigation strategies.

**Keywords:** coastal landslides; mass rock creep; coastal cliffs; land surface analysis; data analysis; Conero promontory

## 1. Introduction

Landslides of different typologies and size can occur along active retreating coastal cliffs, where the gravity-induced processes often superimpose, in space and time, to marine processes in shaping the coastal slopes. Rocky coasts represent about 80% of coasts worldwide [1], and they represent a great part of coasts around the Mediterranean basin [2]. Rocky coasts have been broadly studied so far, representing zones with high economic, social, cultural, and touristic values. In particular, many studies focused on the factors controlling erosional processes along both hard and soft rock coasts [3], whereas other studies focused on the present morphodynamics, with a particular emphasis on the role of active landslides on the present evolution of the coastline and the associated hazards [4,5]. Nonetheless, the understanding of the role of the slope shape and tectonic structures on the long-term morphoevolution of coastal slopes is crucial to enhance the awareness of slope instability on rocky coasts.

Complex morphodynamics, implicating multiscale morphoevolutionary scenarios, often characterize rock slopes affected by extensive landslide processes. Mass Rock Creep (MRC) *sensu* [6], has been demonstrated to represent a critical process for the long-term morphoevolution of rock slopes in different geological contexts [7–9]. Large disruptive landslides may represent the ultimate stage of the MRC process that can culminate in paroxysmal events (like rock avalanches); nevertheless, these ultimate events are anticipated by gravity-driven deformations which represent the strain effect of the rock mass viscous rheology. When these deformations develop into abrupt and generalized slope failures, it is caused by an increasing strain rate over time [10]. In particular, threshold conditions can be reached when the stationary creep stage evolves into an accelerating creep stage [11,12]. Generalized slope failures are typically associated to mass strength reduction due to rock mass damage, the latter occurring over time as an effect of viscous deformation [13,14]. Catastrophic failures that occur in the accelerating stage of MRC process can progress rapidly into rock avalanches and slides that are generally due to the fragmentation of the involved rock masses throughout their propagation and emplacement [15].

Coastal slope processes can be prone to evolve in paroxysmal events [16–18] or can display a continuous slow activity associated with MRC process [19–22]. Along rocky coasts, proneness to landslides needs to consider the relations between the cliff rheology and lithostructural setting, as well as external stresses [23,24], such as rainfall, earthquakes, or storm sea waves. Furthermore, considering the coastal slope instability at a longer time scale, changes in sea level, occurring over a wide range of space–time scales [25], should be taken into account.

The investigation of rocky coasts often represents a research challenge due to the accessibility of rock cliffs in all their portions. Remote sensing techniques from satellite imagery and aerial photos can be sometimes unhelpful due to cliff attitude and/or in the case of high-angle sloping coasts, as for example plunging cliffs. [26] proposes a methodological approach for the continuous acquisition of geological, geomorphological, hydrogeological, and biological datasets along rocky coasts based on a snorkeling approach. The latter is helpful for a detailed mapping of landforms and processes at the foot of the coastal slopes. [27] proposed a combined approach based on snorkeling-based and traditional fieldwork in the inland for a detailed mapping of the rocky coasts affected by gravity-induced slope processes.

The rocky coast at the Conero promontory (Central Adriatic Sea, Italy) presents several features that account for the predisposing role of morphostructural setting on coastal landslide processes involving extensive rock slopes [28,29]. Moreover, this area provides a wide set of geomorphic and tectonic elements that can be regarded as conditioning factors for the MRC process evolution [27].

The main goal of this study consists in unraveling the role of morphostructures as a controlling factor for the coastal morphodynamics and the implication of the latter on the gravity-induced slope processes that act at different spatial and time scales. Different long-term morphoevolutive scenarios are considered based on different geomorphological/structural settings and the possible triggering mechanisms, then their implications on the present-day slope instability are discussed.

## 2. Dataset and Methods

A combination of laboratory- and field-based techniques consisting of land surface quantitative analysis and geomorphological–structural surveys were performed. The topographic dataset, available for the study area in vector format at the scale of 1:10,000, was used as a basemap for the field surveys. These surveys were preliminarily supported by the interpretation of panchromatic orthophotos, available for the years 1988–1989 and 1994–1998 at www.pcn.minambiente.it as a web map service (WMS), together with panchromatic aerial photos available at the scale of 1:33,000 (year 1954) and 1:75,000 (year 1989). Land surface quantitative analysis was performed, starting from a Digital Elevation Model (DEM) with a ground resolution of 2 m and derived from the LiDAR (Light Detection and Ranging) dataset available for the Italian coastline at www.pcn.minambiente.it. A Geographic Information System (GIS) using the ESRI® ArcGIS 10.6 desktop software platform was used for storing geomorphological and geostructural data derived from the surveys, other than for managing the whole dataset and elaborating the quantitative analyses.

### 2.1. Geomorphological and Structural Survey

A series of geomorphological surveys, organized between the spring and summer of 2019, were carried out for corroborating previous surveys [27,30], which mainly focused on coastal processes and landforms, with particular attention on the detection of tidal notches and their morphoevolutive significance. The surveys performed here aimed at refining the recognition and mapping of coastal and gravity-induced processes and landforms, as well as at enlarging this detection along the entire coastal slope between the Portonovo and the Due Sorelle sites (Figure 1).

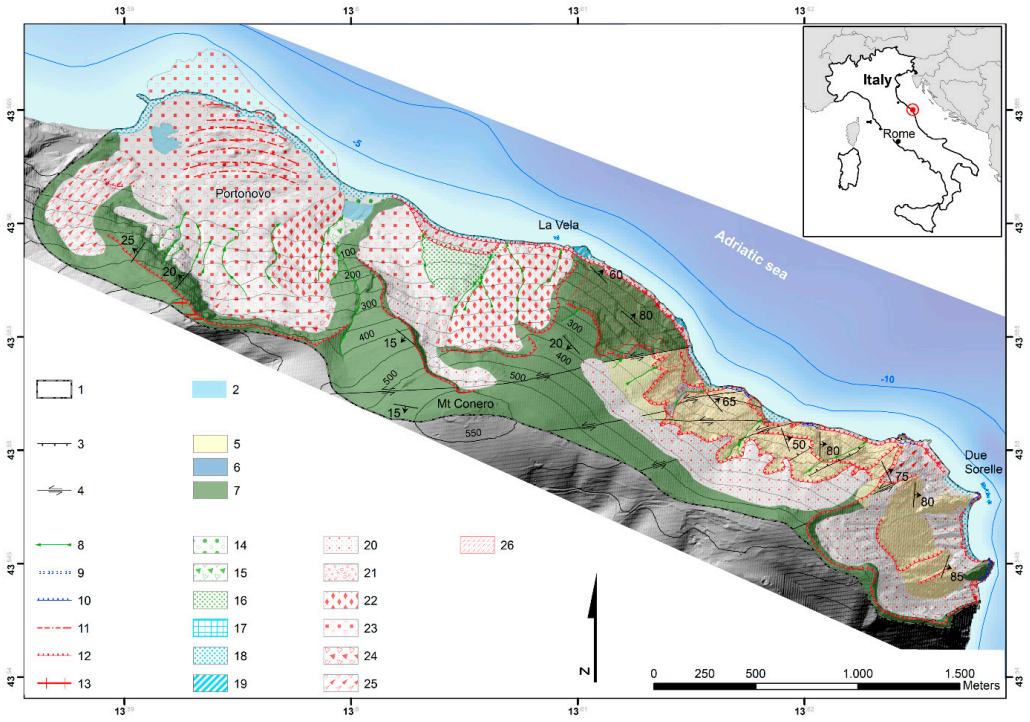


**Figure 1.** Geomorphological map of the Conero promontory showing the main geological and structural elements (map coordinates are in WGS84 cartographic reference system). Near-coast bathymetry (0–10 m below the sea level) is also indicated. 1: study area; 2: lake; 3: normal fault; 4: strike-slip fault; 5: Maiolica Fm.; 6: Marne a Fucoidi Fm.; 7: Scaglia Rossa Fm.; 8: gully erosion; 9: tidal notch; 10: plunging cliff; 11: landslide-toe compressional ridges; 12: rocky scarp; 13: landslide trench; 14: swamp; 15: alluvial fan; 16: stratified slope deposit; 17: sea stack; 18: beach; 19: shore platform; 20: slope debris and talus deposits; 21: debris flow; 22: debris avalanche; 23: rock avalanche; 24: rock fall; 25: rock slide; 26: diffuse gravity-driven slope deformations.

The detection and mapping of the processes and landforms were based on the approach proposed by the new Italian Geomorphological Mapping guidelines [31], which suggest mapping each landform based on its genesis, evolution, and present dynamics. The peculiar amount of landslide phenomena affecting the coastal slopes imposed special attention on the detection and mapping of the gravity-induced processes and landforms, and their complex evolutionary scenarios. Geomorphological fieldwork was preceded by the interpretations of the panchromatic orthophotos visualized in the GIS platform and by the interpretation of the historical aerial stereopair images, which were helpful for a preliminary delimitation of both large landslide bodies and debris deposits. Results of these preliminary tasks were also helpful for tracing the main structural lineaments. The optical satellite images available in Google Earth, together with the ones available in ArcGIS 10.6 (i.e., TerraColor dataset) were consulted for planning fieldwork and for supporting the mapping of the largest landslide features, other than for delimiting the main cliff escarpments. The multitemporal remote sensing analysis was also useful for defining the recent activity of the main landslides. After the geomorphological fieldwork, final refining of the geomorphological mapping was completed through the 3D visualization of the topography at high-resolution, thanks to a hillshade map derived from the 2 m-cell-sized DEM in the GIS platform.

Geostructural surveys, conducted together with the geomorphological ones, were carried out to detect and characterize the main tectonic structures that strongly control the rock mass behavior, as well as for refining the mapping of the lithological units composing the bedrock. The final aim was to unravel the connection between the local bedrock discontinuity frequency and distribution and the rock slope deformation and instability.

The fieldwork was conducted using digital survey techniques, based on mobile devices that allowed for collecting field data in digital form, and its direct storage through remote cloud-uploading and real-time updating.

### 2.2. Land Surface Quantitative Analysis

The objective classifications of terrain types, at the base of the quantitative geomorphic analysis, require the use of both local and statistical terrain parameters helpful for defining the topographic signature of different surface processes and landforms [32]. Nonetheless, given the strong variability of landforms in size and tridimensional shape, due to different morphogenetic factors, many terrain parameters have been proposed to provide a quantitative description of topography [32,33]. In this research, two main geomorphometric parameters were selected among numerous DEM-based terrain parameters, considering the specific research aim as well as the spatial scale of the analyses performed. The selected parameters were calculated starting from the available 2 m-cell-sized DEM.

The first parameter is the slope angle, derived by means of the surface slope algorithm running in the Spatial Analyst extension of the GIS platform. For each DEM cell, this algorithm computes the first derivative of the elevation surface, or the maximum change in elevation between a cell and its eight neighbors (i.e., the steepest downhill descent from the cell) [34].

The second parameter is the surface roughness that can be successfully used to define different landslide features and to examine the landslide activity [35,36]. Different methods have been proposed to compute the surface roughness [37–39], although one of the most used methods is simply based on the statistical dispersion of heights or slopes. In this work, the surface roughness was calculated as the standard deviation of the elevation values within a $4 \times 4$ moving window. This method, among many calculation methods revised by [36], was demonstrated as one of those useful for evidencing the topographic signature of large landslides. In order to obtain the surface roughness values, the focal statistics tool running in the ArcGIS 10.6 platform was adopted.

For supporting the spatial interpretation of both parameters, color-coded maps were produced and superimposed with a hillshade map, thus favoring the visualization of both terrain morphology and the spatial variation of parameters. Descriptive statistics for both parameters were calculated and reported as an inset for each map. Finally, for both parameters the number of pixels per bin

(i.e., pixels in each parameter class) was reported using separate histograms for the southern and northern coastal sectors.

A composite altimetric profile parallel to the coastline was created, starting from the 2 m-cell-sized DEM. This composite profile reports the elevation distribution for progressive distance along three different tracks, thus allowing for a more accurate description of coastal morphology. The first track permits delineation of the cliff escarpment morphology (i.e., upslope zone); the second track favors the description of the morphology along the intermediate slope portion (i.e., midslope zone); and the third track portrays the base of the coastal slope, at about 50 m in from the present shoreline (i.e., footslope zone). The extraction and visualization of both slope angle and surface roughness values along two distinct transects support the study of the distribution of these parameters along different portions of the slope. This visualization increases the evidence of parameter value variation due to the presence of landslides of different type, size, and state of activity. The parameters were extracted along the midslope zone (i.e., at the +200 m a.s.l. contour line) and along the footslope (i.e., at the +20 m a.s.l. contour line).

## 3. Study Area

The Conero coastal sector stretches for about 5 km along the Adriatic Sea in the Central Italy, 10 km SE of the Ancona city, and represents its inflection point. Mt. Conero (43°33′04″ N, 13°36′18″ E) constitutes the highest relief along the Adriatic coast with an altitude of 572 m a.s.l. (Figure 1). The climate is of the Mediterranean type with mean annual precipitation of 780–790 mm and mean annual temperature of 14–15 °C. Summers are generally hot and dry, though a marked variability characterizes winters, mostly depending on the Atlantic cyclogenesis [40]. Prevailing winds approach from the SSE–SSW sectors [30] and account for the dominant SE main wave direction. During the winter months, sea-storm waves up to 3–3.5 m and with NE secondary wave direction can strike the coastline, during Bora wind conditions. The average tidal range in the Conero area is about 0.5 m and the action of tidal current is extremely low [27].

Concerning the geological setting, the Conero promontory consists of an asymmetric, NE–E verging anticline with NNW–SSE axial directions [29,41] and represents the easternmost outcropping part of the external stack of the Umbria–Marche foreland fold and thrust belt.

Limestones and marly calcareous terrains compose the bedrock of the study sector of the Conero promontory and are ascribable to the Umbria–Marche stratigraphic succession, from Cretaceous to Oligocene [29]. The complete stratigraphic sequence consists of the following formations, from oldest to youngest: Maiolica Formation (Fm.) (MA; Lower Cretaceous; prevalently composed of decimetric well-stratified limestones with chert and black shales), Marne a Fucoidi Fm. (MF; Lower Cretaceous; prevalently composed by centimetric marls and marly calcareous layers with black shales), and Scaglia Rossa Fm. (SR; Upper Cretaceous; composed of alternating and well-stratified centimetric to metric limestones, calcarenites, biocalcarenites and marly calcareous layers). In the area, this stratigraphic sequence presents some peculiarities with respect to the outcropping in the internal area of the Apennine chain. In particular, the thickness of the MF is about 15 m, whereas the regional thickness is generally up to 80 m. Furthermore, the paraconformity erosive contact between the MF and SR formations is likely caused by syn-sedimentary slumps [42]; in fact, in the area, the Scaglia Bianca Fm. together with a part of the basal portion of the Scaglia Rossa Fm. is totally absent [27]. The western side of the Mt. Conero anticline is gently dipping (around 25°) and affected in the inner part by N–S right-lateral transtensive strike-slip faults with an offset of hundreds of meters. The eastern, coastward flank of the Conero asymmetric anticline is strongly inclined and is intersected by several transversal left-transtensive faults with an average E–W direction and offset a few km (Figure 1). The shear zones are characterized by cataclastic deformation, often with calcite veins and a thickness up to a few meters. The joint pattern is well developed in the rock masses with three prevalent directions NE–SW, NW–SE, and E–W. A pervasive cleavage with subvertical SW dipping planes is observable especially in the Maiolica and in the calcareous Scaglia Rossa bedding. Subhorizontal diagenetic

stylolites are quite common in the Maiolica Fm. Subvertical joints are developed mainly in the Scaglia Rossa Fm., with systems striking NW–SE and ENE–WSW, associated with breccias in related shear zones and systematic calcite veins.

The morphogenesis along the coastal slope is mainly conditioned by gravity-induced and marine processes, with the corresponding landforms and deposits (Figures 1 and 2). Landslides of different typologies, size, and state of activity are widespread in the area and principally characterize the entire coastal slope morphodynamics (Figure 1). Among the main mass movements, the landslides occurring in the northern coastal sector, at Portonovo and La Vela, are the largest ones (Figures 1 and 3A) [29]. Along the coastline, landslide deposits and plunging cliffs interrupt the poorly developed beaches and pocket beaches. The latter mainly consist of rocky blocks and gravels. Flat shore platforms, slightly inclined seaward, are also observable. Typical sea stacks at La Vela and Due Sorelle are located at short distances from the coastline (Figure 2). The current tidal notch occurs around these sea stacks [27]. The absence of either hanging or uplifted tidal notches, together with the absence of Tyrrhenian marine deposits and terrace remnants, testify of an active and intense morphodynamic in the entire coastal slope [27], mainly due to gravity-induced processes and the interrelated factors, such as geological factors or climate variations [43]. Several anthropic structures and man-made landforms, such as a local harbor, some touristic infrastructure, and parking areas, appear at the Portonovo landslide toe, close to the coastline.


**Figure 2.** Main landforms due to coastal processes at the foot of the cliff. (**A**) Shore platform along the central sector of the study area. Calcareous boulders due to recent rock falls are visible in the emerged portion of the platform. (**B**) Due Sorelle sea stacks and the adjacent pocket beach along the southern coastal sector.

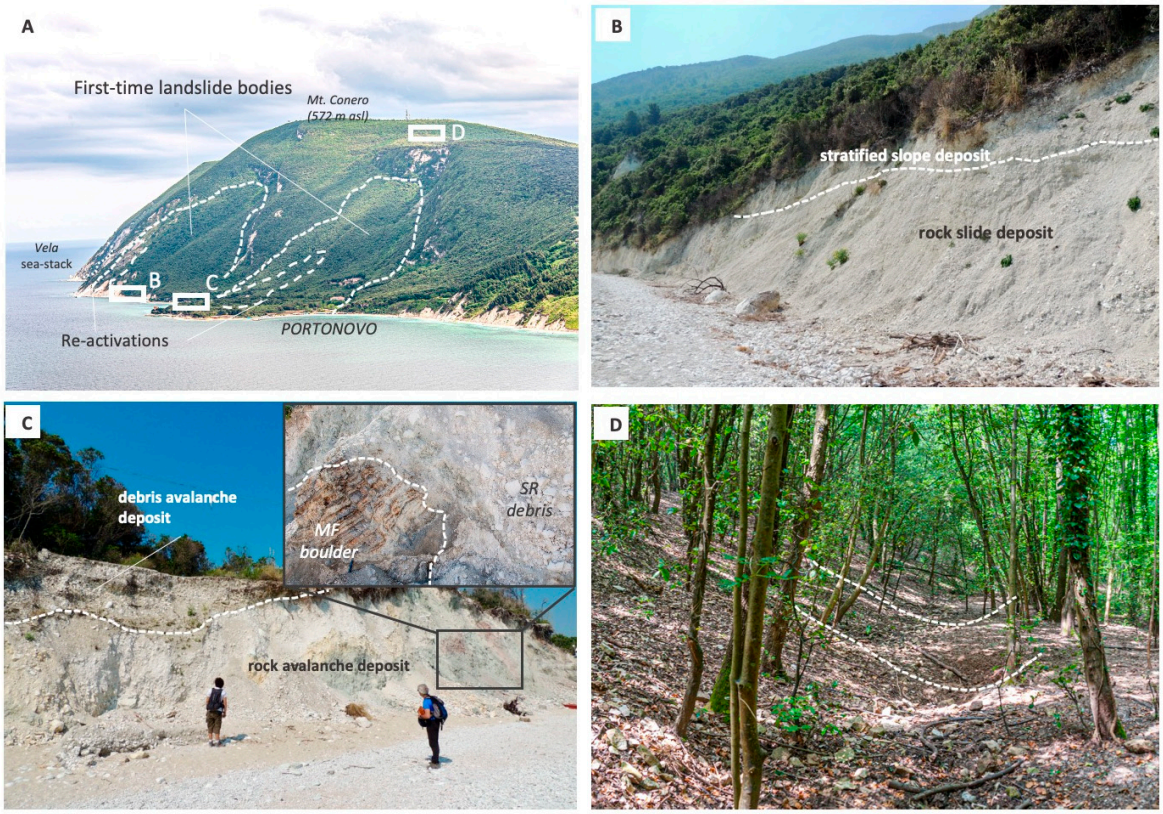


**Figure 3.** Landforms and deposits due to gravity along the northern portion of the Conero rocky coast. (**A**) Panoramic view, towards the south, of the Portonovo and La Vela rocky coast (northern coastal sector). **(B)** Toe area of the Vela rockslide. In this sector, a late-glacial stratified slope deposit (i.e., èboulis ordonneè) overlays the landslide deposit. (**C**) Rock avalanche deposit at the toe of the Portonovo landslide exposed along a wave-cut scarp. The inset shows chaotic debris prevalently belonging to the Scaglia Rossa Fm. (SR) and incorporating a marly calcareous boulder belonging to the Marne a Fucoidi Fm. (MF). (**D**) Ridge-top depression in the Portonovo landslide backscarp area.

## 4. Results

The Conero promontory provided a set of data useful for better defining the morphoevolutive implications of the gravity-induced processes and landforms along the coastal zone. The entire coastal slope is affected by landslides of different typologies, which account for erosional landforms at the upslope zone and abundant landslide deposits along the mid- and footslope sites (Figure 1, Figure 2A, Figure 3, and Figure 4). Landslides are predisposed by low persistency of rock mass joints and by strata attitude whose dip is very close to the slope face direction.

The largest mass movements surveyed in the area occur in the northern coastal sector, between the Portonovo village and the La Vela sea stack (Figure 1), where two adjacent, large landslides masses can be observed and ascribable to rock-avalanche/slide mechanism [44], as they are associated with wide detachment scars that typify the sharp edge of the coastal cliff and delimit seaward the calcareous ridge top (Figures 1 and 3A). The northern landslide (Portonovo landslide) shows a runout of about 500 m that flowed seaward, accounting for the shaping of a bay where Portonovo village developed. A series of typical compressional ridges characterize the distal zone of this mass movement. The southern landslide (La Vela landslide), on the contrary, shows a truncated toe, though observing the trend and geometry of the contour lines down to −10 m b.s.l., the nearshore morphology of the seafloor indicates that a terminal landslide lobe is still detectable (Figure 1).


**Figure 4.** Landforms and deposits due to gravity along the southern portion of the Conero rocky coast. (**A**) Panoramic view of the Due Sorelle cliff. Falls and slides of rock blocks occur in the uppermost cliff portions, characterized by a sharp subvertical escarpment. Bedding attitude coincides with topography along the intermediate slope portion. At the cliff base, thick talus deposits occur, often interested by small debris flows and falls. (**B**) Evidence of a rock-fall detachment zone along the main cliff escarpment.

Patches of a thin layer of stratified slope-waste deposits form outcrops along the cliff base (Figures 1 and 2B) and unconformably overlay the chaotic landslide deposits. Stratified slope deposits are widespread within the Umbria–Marche Apennines, even along the coastline [45], principally where bedrock particularly prone to frost shattering, as Maiolica and Scaglia Rossa formations, is exposed. These deposits typify cold, periglacial environments [46] and represent in the Apennine area the termination of the last glacial slope–fluvial sedimentation cycle [47], thus their chronological collocation is at the end of Late Pleistocene [48].

A characteristic wave-cut scarp parallel to the present shoreline delimits the toe of both the landslide masses and provides suitable exposures of the deposits that here are those typical of rock avalanche/slide phenomena: disrupted rock masses, including rock blocks; chaotic calcareous debris with sandy clay; and a subordinately clay matrix (Figure 3B,C). Rock blocks and calcareous debris belong to the Scaglia Rossa Fm. and subordinately to the Marne a Fucoidi Fm., confirming that both bedrock formations are involved in the mass movement. At the toe of the Portonovo landslide, a deposit belonging to a shallow reactivation of the main landslide body uncomfortably overlays the rock avalanche/slide deposit (Figure 3C). Along the backscarp of both landslides, a series of trenches and ridge-top depressions mark the releasing zone (Figure 3D).

A plunging cliff characterizes the southern coastal sector, whose upslope and midslope zones are generally affected by rock-block slides and falls that strongly contribute to the cliff regression (Figure 4). A wide active talus deposit occurs at the footslope, often affected by secondary debris flows and fall phenomena. The main instability of the coastal cliff is strictly controlled by lithostructural factors, and just a few and limited zones along the cliff are subjected to the prevailing action of undercutting due to the sea actions.

Location and scale of gravity-induced instability processes appear related to the structural settings of the Mt. Conero anticline; in the southern sector, NE-dipping, high-angle bedding conditions the rock mass stability, providing the kinematic arrangement for planar and wedge-sliding, which seasonally affect the coastal slopes by mobilizing block volumes from tens up to hundreds of cubic meters. The repeated rock-block instabilities feed the slope system with a large amount of detritic material, which is mobilized by channelized flows after intense rainfalls.

The northern sector is instead featured by an E–ENE dip direction of bedding, resulting from fold-axis plunging and periclinal folding, as identifiable in the east escarpment of the Portonovo landslide. In this area, high-angle preorogenic transtensional faults [41] dissected the anticline forelimb, providing the inherited passive framework where slope-scale deformation evolved [49,50].

Evidence of slope-scale, gravity-driven processes occur along the entire coast where mesoscale features of MRC processes were surveyed (Figure 5).

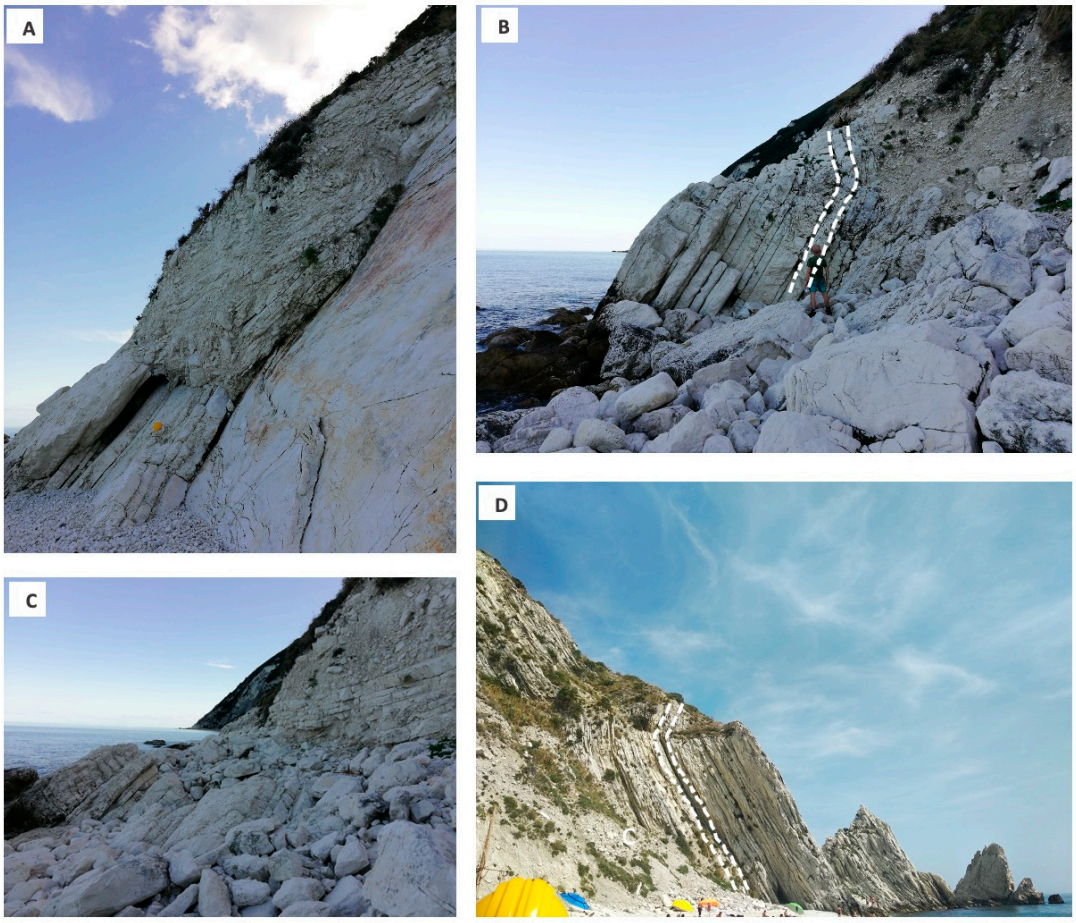


**Figure 5.** Evidence of ongoing gravity-induced deformations along the coastal slope due to the MRC process. (**A**) Buckling folds affecting the calcareous layers at the Vela cliff. **(B**) Flexural toppling south of the Vela cliff. (**C**) Rock fall due to a buckling fold breakout. (**D**) Flexural block-toppling at the Due Sorelle cliff.

The structural observations indicate macroscopically ductile features of slope-scale flexural toppling along a steeply dipping and narrow-spaced primary discontinuity set, despite the presence of horizontal cross joints. The latter act as a breakout surface, driving the relative rotation of blocks with respect to a defined hinge surface [51]. These observations lead to a challenging distinction between flexural-toppling and brittle block-toppling [52], thus suggesting a transitional behavior strongly dependent on local lithological and joint density properties of the rock masses. Buckling folds also affect the calcareous bedding at the Vela cliff, causing tension and shearing fractures that can enhance the occurrence of rockfalls.

Along the analyzed coastal slope, the slope angle parameter shows a wide range of values (i.e., 0–88°) and its spatial distribution is good evidence for the subvertical geometry of the upslope zone of the cliff (Figure 6A). In particular, the slope map reveals a very good match between the maximum values and the main rock-block detachment zones and the large landslide scar areas, respectively, in the southern and northern coastal sector. In the latter sector, the lowest slope angle values also appear at the foot of the cliff, delimiting the Portonovo landslide toe. Statistics show the prevalence of the highest slope values in the southern sector (Figure 6B), while within the northern sector, the values are distributed heterogeneously (Figure 6C) with a prevalence of the lowest values at the foot of the cliff (Figure 6A,C).

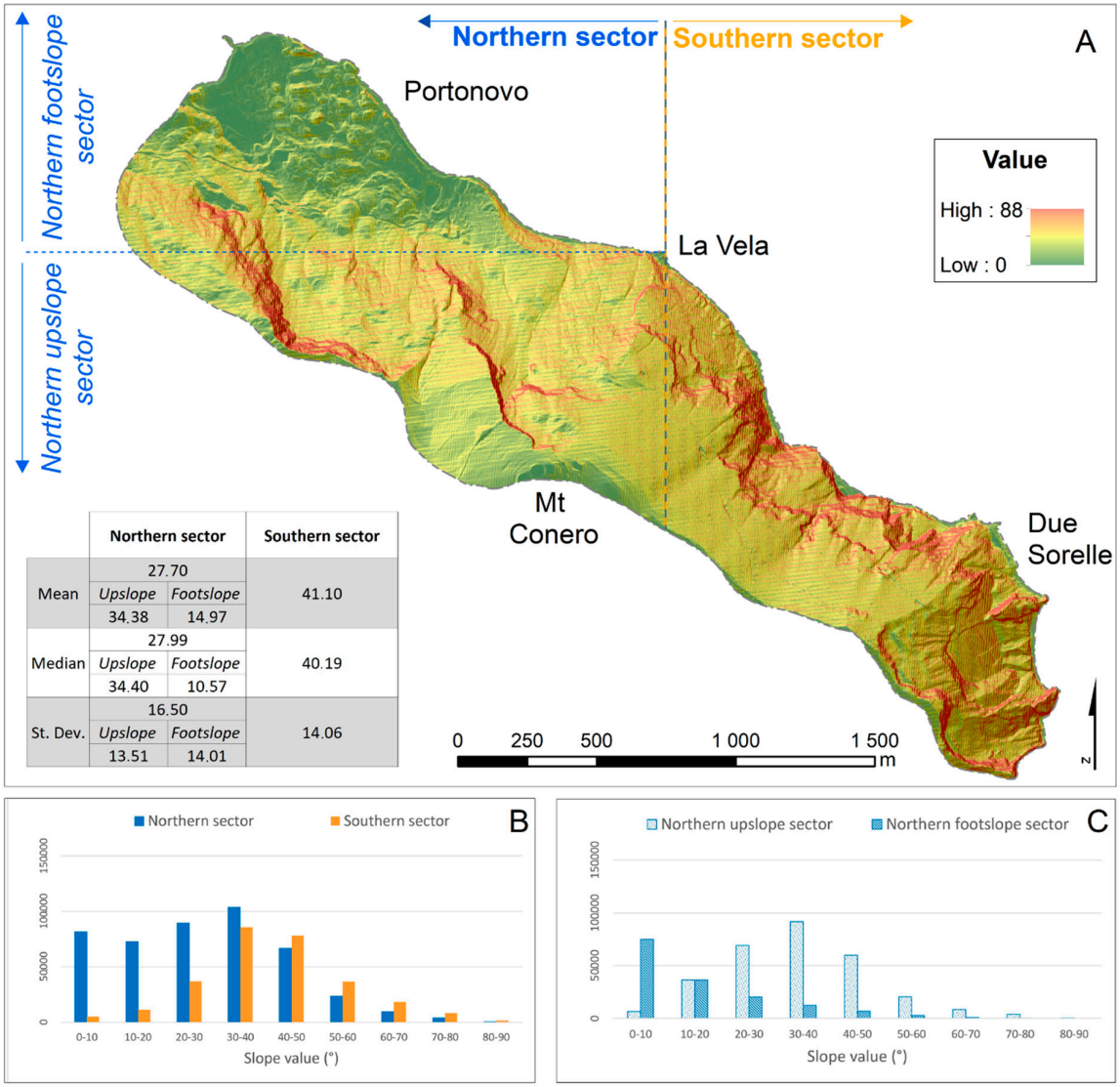


**Figure 6.** Spatial distribution of the slope values in the study area, based on a LiDAR-derived elevation dataset with ground resolution of 2 m. (**A**) Color-coded slope map overlain with a hillshade map, including a table with descriptive statistics. (**B**) Histogram with the distribution of slope values within the southern and northern sectors of the study area (y-axis reports the number of pixels per bin). (**C**) Histogram with the distribution of slope values within the footslope and upslope portions of the northern sectors of the study area (y-axis reports the number of pixels per bin).

The surface roughness parameter shows values up to 33 m (Figure 7). The highest values occur along the main rocky scarp, whereas the lowest ones occur in more homogeneous, flat or smoothed zones. The zones with the highest roughness coincide well with the ones with the highest slope values, along the main detachment areas for the rock-block falls. As for the slope parameter, even the surface roughness permits delineation of two almost homogenous zones along the coastal slope. The southern sector shows the largest values, while average small values are recorded in the northern sector (Figure 7B). More in detail, within the northern sector two distinct zones can be distinguished, based on surface roughness (Figure 7C). The first zone, involving the entire body of the La Vela landslide and the upper zone of the Portonovo landslide, rests within the base of the scar area downhill to the upper termination of the toe. The second zone coincides with the Portonovo landslide toe. This particular configuration is easily recognized along the transect at +200 m a.s.l. (Figure 8). This latter zone, along its northern portion shows similar values that range between 3 and 6 m; more in

detail, the values are the same where the transect crosses both the La Vela and Portonovo landslide bodies (Figures 1, 3A and 9). Along the transect at +20 m a.s.l., on the contrary, the roughness values are dissimilar for the toe areas of the two adjacent landslides, with the La Vela foot zone showing the same values as the uppermost transect and the Portonovo footslope zone showing lesser values. The highest roughness values occur along the transect at +20 m a.s.l. along the southern coastal sector, marking well the topographic setting of the base of the active retreating cliff.

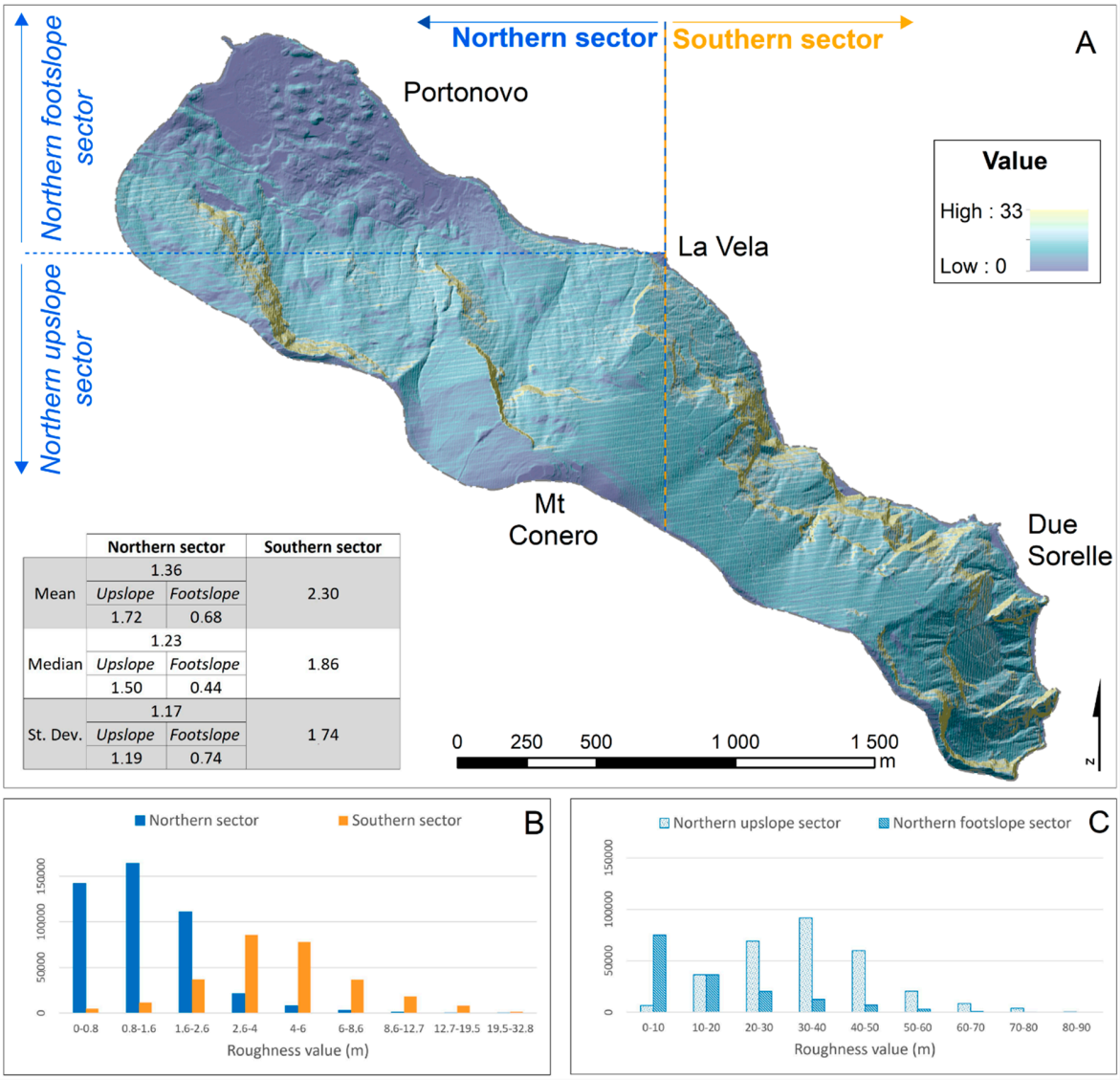


| | Northern sector | | Southern sector |
|---|---|---|---|
| Mean | 1.36 | | 2.30 |
| | *Upslope* | *Footslope* | |
| | 1.72 | 0.68 | |
| Median | 1.23 | | 1.86 |
| | *Upslope* | *Footslope* | |
| | 1.50 | 0.44 | |
| St. Dev. | 1.17 | | 1.74 |
| | *Upslope* | *Footslope* | |
| | 1.19 | 0.74 | |

**Figure 7.** Spatial distribution of the surface roughness values in the study area. (**A**) Color-coded surface roughness map overlain with a hillshade map, including a table with descriptive statistics. (**B**) Histogram with the distribution of surface roughness values within the southern and northern sectors of the study area (y-axis reports the number of pixels per bin). (**C**) Histogram with the distribution of surface roughness values within the footslope and upslope portions of the northern sectors of the study area (y-axis reports the number of pixels per bin).

The quantitative analyses performed by means of altimetric profiles in the coastline direction improved the interpretation of the outcomes described above, as well as allowed the definition of the different topographic and geometric characteristics of the analyzed southern and northern sectors, and the ones of the upslope and midslope zones (at +200 m a.s.l.), and the footslope (at 50 m from the present shoreline).

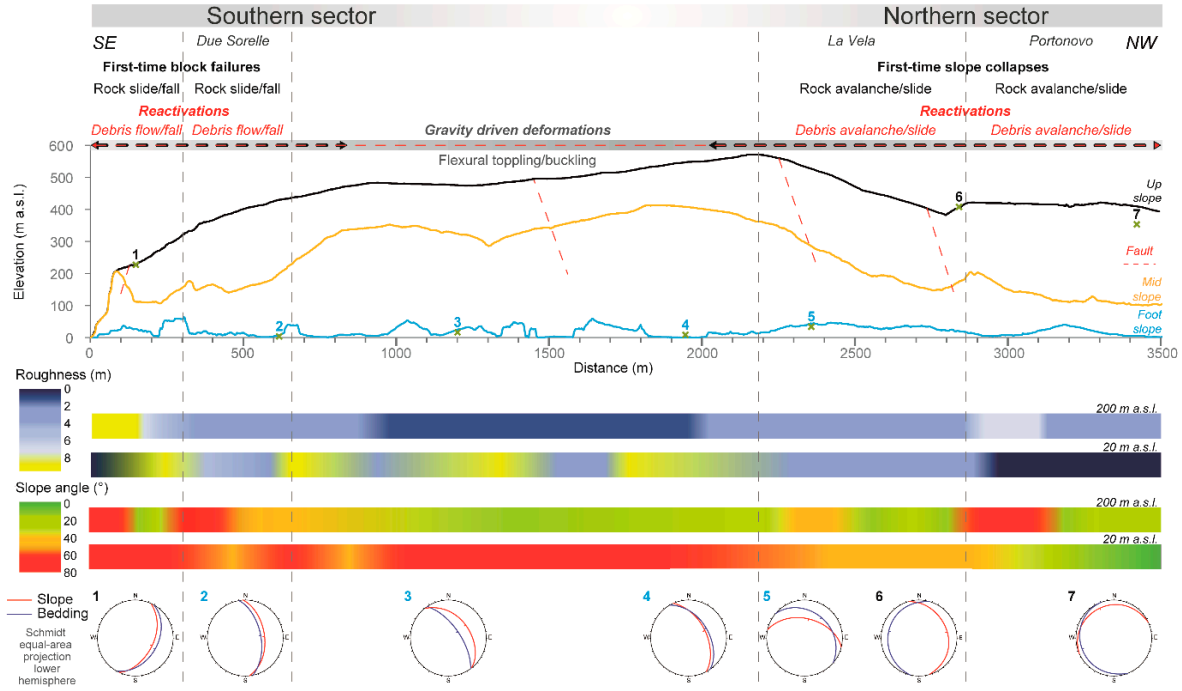


**Figure 8.** Composite altimetric profile of the entire coastal slope. The three superimposed profiles illustrate the morphology of the upslope, midslope, and footslope zones (the latter at 50 m in from the present shoreline). For the principal geomechanics measurement positions, the stereo plots illustrate the bedding attitude with respect to the slope geometry (topographic steepest descent). Below the profiles, the variations of both slope angle and surface roughness along the two distinct transects at the elevation of +20 and +200 m a.s.l. are reported.

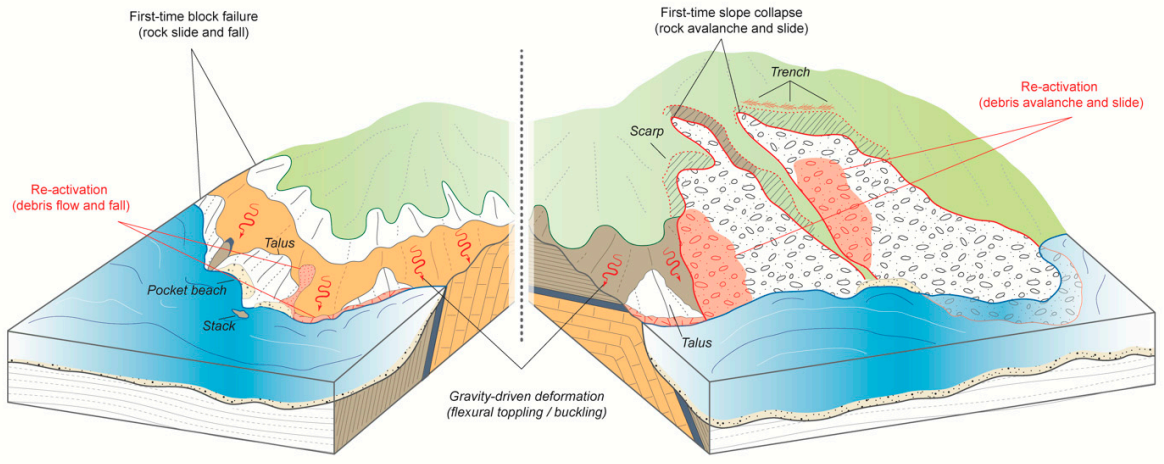


**Figure 9.** Conceptual landscape model. The 3D sketch illustrates the different morphodynamic styles characterizing the southern (left sketch) and northern (right sketch) coastal sectors. Morphostructural settings strongly influence the types and development of different gravity-induced processes, as well as diverse landform associations and their spatial organization and evolution at different scales. Slope-scale, MRC-driven processes dominate the long-term morphoevolution of the northern coastal sector, whereas the southern sector is generally characterized by cliff-scale, force-driven processes. See Figure 10 for further details.

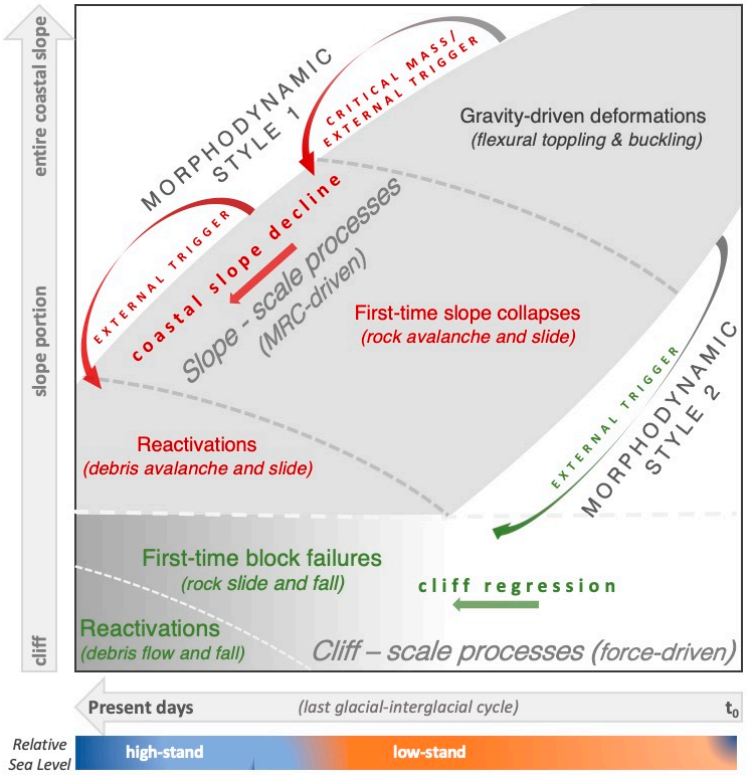


**Figure 10.** Conceptual space–time evolutive model for the active retreating coastal slope along the Conero promontory. Starting from the same process affecting the entire coastal slope, different long-term morphoevolutive scenarios are expected, depending on two different morphodynamic styles. The first scenario refers to slope-scale, time-dependent processes, while the second one refers to cliff-scale, time-independent (i.e., force-driven) processes. Both scenarios coexist along the analyzed coastal slope. The first one is typical of the northern coastal sector, where it favors active coastal slope downward erosion; the second scenario prevails along the southern coastal sector, where it accounts for active cliff regression.

The distribution of the slope parameter along the transect at +200 m a.s.l. (Figure 8) displays similar values, generally not exceeding 40–45° with two major exceptions at the Due Sorelle cliff, in the southern sector, and at the right flank of the Portonovo landslide, in the northern sector. Except for the Portonovo landslide toe zone (Figure 3A), where the average slope values are below 20°, along the transect at +20 m a.s.l. the average slope values are >40–45° (Figure 8), highlighting the presence of a high-angle or subvertical active retreating cliff (Figures 2A and 9). The +20 m transect crosses either the base of the rocky slope or the talus deposits at the footslope in those sectors where it occurs (Figure 4).

## 5. Discussion

Two distinct sectors can be recognized along the Conero slope, typified by convex, dip-slopes [53]. The first one includes the northern sector embracing the Portonovo and La Vela zones, whereas the second sector encompasses the whole southern portion of the coastal slope at the Due Sorelle sea stacks. The two slope portions, featured by the same geological formations, show many differences in both topographic (Figure 8) and structural settings (Figures 8 and 9). Consequently, these sectors experienced different morpho-evolutive styles due to gravity-induced processes acting at different space- and time scales (Figure 10). In the northern portion of the area, at the slope scale, massive rock slope failures and their related scar areas mainly characterize the landscape of the coastal area, whereas cliff-scale, rock fall, and rock slide typify the landforms along the southern sector.

It is reliable to assume that a first-time massive rock slope failure, representing the generalized slope collapse as the final stage of the MRC process, characterizes the entire slope encompassing both

Portonovo and La Vela localities with an estimated volume of about $40 \times 10^6$ m$^3$. The latter likely developed in at least two steps (i.e., multistep first-time event): the first one involving the whole coastal sector and the second one only the Portonovo coastal slope. Both events likely occurred during the last glacial time. The lack of remnants of the marine terrace representing the Middle Pleistocene highstand [27] and the presence of the periglacial deposits sealing the main landslide bodies both support this assumption. Moreover, the relative freshness of the landslide-related erosional and depositional landforms allows exclusion of the collocation of the mass movements during earlier glacial cycles. The spatial distribution of surface roughness values along the northern coastal sector seems to confirm that the two landslide bodies belong to the same first-time event, and that only the Portonovo area experienced a second massive rock slope failure event. In fact, the La Vela landslide body shows nearly the same roughness values as the upslope portion of the Portonovo landslide, indicating a similar postevent remodeling, hence the same timing. Both landslide bodies were partially reactivated during historical time (mainly debris avalanche/slide phenomena) and field evidence confirms this observation, especially at the Portonovo locality. At this location, a catastrophic large landslide event occurred during the Middle Ages, destroying the local harbor and an ancient Benedictine Abbey [29].

From an evolutive point of view, the Conero coastal slope can be considered a typical palimpsest landscape (*sensu* [54]), where landforms belonging to the same process that make up the landscape (the gravitational one in the present case) developed at different spatial scales, have different age and, at present, display dissimilar dynamics. In fact, the nested landslide system that characterize the Portonovo and La Vela coastal slope likely started to develop during the beginning of the last glacial time, under cold environmental conditions and relatively low sea level (only the surficial landslide reactivations, though catastrophic, developed under the present environmental conditions). This morphodynamic style accounts for the down-wearing evolution of the rocky coast, with the upslope portion eroding downward as the footslope receives the supply of upslope sediments and advances seaward (Figures 8 and 9). On the contrary, the southern sector is a typical active plunging cliff, whose morphodynamic style, though dominated by the gravity-induced processes, is in part actively related to the coastal processes due to continuous sea wave action, tidal range, and storm waves, in particular along the footslope portions. Rock-block slides and rockfalls dominate the upslope portion accounting for the upper escarpment retreat, whereas at the base of the coastal slope, in addition to rock-block falls and slides, debris flows and falls also account for the cliff retreat. Several earthquake-induced landslides were reported for this portion of the Conero promontory [55], often triggered by the low-magnitude, high-frequency seismic events that typically characterize the seismicity of the external portions of the Apennine chain.

It is assumed that the dominant role of the different morphoevolutive styles along the Conero coastal slope is strictly related to the different structural settings (Figures 8 and 9) that account for the rather different development of MRC processes.

A double scale morphodynamic conceptual scheme is proposed in Figure 10, where time is reported on the x-axis and space on the y-axis. According to the time scale, the processes considered evolve from gravity- to force-driven during recent times, as these processes involve more limited portions of slopes, causing smaller size landslide events. These last events can be triggered by time-independent local and transient forcing, such as sea storms and earthquakes, while the larger size rock mass failures (i.e., rock avalanches and slides), which can be observed in the northern sector of the Conero promontory, are substantially triggered by inertial forces as they result from MRC, causing viscous deformations over time (red arrows in the conceptual scheme, Figure 10). For a higher dip of strata attitude, the MRC deformations (occurring at the entire coastal slope scale) do not envelop critical volumes that can become prone to failure over a longer time [7]; in this last condition, the morphoevolution results in several small-size failures (occurring at the cliff scale), which are represented principally by the rock-falls and slides in the southern sector of the Conero promontory (green arrows in the conceptual scheme, Figure 10). Reactivations are also possible, after initial mass rock failures, due to debris avalanche/slide or debris flow occurrence. Concerning the

climatic context and referring to the last glacial–interglacial cycle, the low-stand phase corresponded to the gravity-driven deformations evolving toward failures, while the high-stand phase mainly corresponds to the cliff-scale processes. The implications of this conceptual model in terms of risk are related to a higher probability of occurrence for the cliff-scale processes, acting at an entire slope scale, which represent the most hazardous ones with respect to the gravity-driven MRC deformations and failure.

The coexistence of large-scale MRC deformational processes and small-scale, time-independent failures is clearly visible in the Due Sorelle sector (southern portion of the Conero promontory) where observation of flexural toppling and buckling demonstrate that progressive rock mass deformations rapidly evolve toward failure (i.e., either falls or slides), thus avoiding larger volumes involving creep processes that reach the critical size for a generalized slope collapse.

Traditional field-based surveying and mapping with quantitative geomorphic analyses based on a high-resolution digital elevation dataset were integrated to represent a more suitable tool for better defining the morphostructural setting of the area under investigation, even in those sites where the field surveys were difficult to perform. DEM-based quantitative land surface analysis, thanks to different visualization techniques and the computation of two geomorphometric parameters, revealed a high-performance mapping methodology that allows for rapid completion of the time-consuming traditional techniques used in refining the survey and mapping slope processes and landforms due to gravity.

Results of this research can be valuable for coastal landslide analysis and propose a conceptual scheme for assessing and monitoring the current dynamics of slopes affected by mass movements of different typologies and size. In particular, this research reveals the importance of the evaluating the long-term morphoevolution of the entire slope for better comprehending the present activity and future development of the coastal landslides.

## 6. Conclusions

Based on field evidence, MRC processes involve the entire coastal slope along the Conero promontory. The coastal slope can be zoned into two distinct sectors, depending on different morphostructural settings and consequent rock slope instability processes. For the long timescale, two separate morphodynamic styles can be delineated along the coastal slope, which are each associated with specific evolutionary scenarios. The first scenario represents MRC-driven, time-dependent slope processes acting at the slope scale, whereas the second one includes force-driven, time-independent slope processes acting at smaller space–time scales. First-time rock slope failures (i.e., rock avalanche/slide mechanism) characterize the northern area of the promontory, which is interpreted as the result of extensive, multistep catastrophic failure that occurred at the final stage of the MRC process. Shallower landslides (i.e., debris avalanche/slide) can locally reactivate the main landslide masses. First-time rock-block slides and falls, occasionally triggered by earthquakes and/or storm sea waves, occur mainly along the southern sector of the coastal slope where they account for the active cliff retreat.

The present study highlights that slope shape and geostructural conditions of deforming slopes are concurrent in allowing the critical volumes for failures to be reached, thus inducing generalized slope collapse that can be regarded as the ultimate stage of MRC processes.

The findings discussed here also confirm the relevance in understanding the role of geomorphological vs. structural features as predisposing factors for slope collapse along rocky coasts. Moreover, the assessment of long-term slope instabilities allows for a better comprehension of the present-day, gravity-induced slope dynamics, suitably supporting landslide monitoring strategies and appropriate mitigation strategies even based on stress-strain time-dependent numerical analyses.

**Author Contributions:** Conceptualization, F.T. and S.M.; methodology, F.T. and S.M.; validation, M.M.; laboratory analysis, D.T. and G.M.M.; field investigation, F.T., D.P., M.M. and D.T.; data curation, G.I.; writing—original draft preparation, F.T., S.M., G.M.M. and D.P.; visualization, D.P. and G.I. All authors have read and agreed to the published version of the manuscript.

**Funding:** This research received no external funding.

**Conflicts of Interest:** The authors declare no conflict of interest.

## References


1. Sunamura, T. *Geomorphology of Rocky Coasts*; Wiley: New York, NY, USA, 1992.
2. Furlani, S.; Pappalardo, M.; Gomez-Pujol, L.; Chelli, A. The rocky coasts of the Mediterranean and Black Sea. In *Rock Coast Geomorphology: A Global Synthesis*; Kennedy, D.M., Stephenson, W.J., Naylor, L.A., Eds.; Geological Society: London, UK, 2014; Memoirs 40; pp. 89–123.
3. Miccadei, E.; Mascioli, F.; Ricci, F.; Piacentini, T. Geomorphology of soft clastic rock coasts in the mid-western Adriatic Sea (Abruzzo, Italy). *Geomorphology* **2019**, *324*, 72–94. [CrossRef]
4. Soldati, M.; Maquaire, O.; Zezere, J.L.; Piacentini, D.; Lissak, C. Coastline at risk: Methods for multi-hazard assessment. *J. Coast. Res.* **2011**, *61*, 335–339. [CrossRef]
5. Gibson, A.D.; Culshaw, M.G.; Dashwood, C.; Pennington, C.V.L. Landslide management in the UK—The problem of managing hazards in a 'low-risk' environment. *Landslides* **2013**, *10*, 599–610. [CrossRef]
6. Chigira, M. Long-term gravitational deformation of rocks by mass rock creep. *Eng. Geol.* **1992**, *32*, 157–184. [CrossRef]
7. Esposito, C.; Martino, S.; Scarascia Mugnozza, G. Mountain slope deformations along thrust fronts in jointed limestone: An equivalent continuum modelling approach. *Geomorphology* **2007**, *90*, 55–72. [CrossRef]
8. Della Seta, M.; Esposito, C.; Marmoni, G.M.; Martino, S.; Scarascia Mugnozza, G.; Troiani, F. Morpho-structural evolution of the valley-slope systems and related implications on slope-scale gravitational processes: New results from the Mt. Genzana case history (Central Apennines, Italy). *Geomorphology* **2017**, *289*, 60–77. [CrossRef]
9. Delchiaro, M.; Della Seta, M.; Martino, S.; Dehbozorgi, M.; Nozaem, R. Reconstruction of river valley evolution before and after the emplacement of the giant Seymareh rock avalanche (Zagros Mts., Iran). *Earth Surf. Dynam.* **2019**, *7*, 829–947. [CrossRef]
10. Vick, L.M.; Böhme, M.; Rouyet, L.; Bergh, S.G.; Corner, G.D.; Lauknes, T.R. Structurally controlled rock slope deformation in northern Norway. *Landslides* **2020**. [CrossRef]
11. Saito, M. (1969) Forecasting time of slope failure by tertiary creep. In Proceedings of the 7th International Conference on Soil Mechanics and Foundation Engineering, Mexico City, Mexico, 29 August 1969; pp. 677–683.
12. Petley, D.N.; Allison, R.J. The mechanics of deep-seated landslides. *Earth Surf. Proc. Land.* **1997**, *22*, 747–758. [CrossRef]
13. Eberhardt, E.; Stead, D.; Coggan, J.S. Numerical analysis of initiation and progressive failure in natural rock slopes-the 1991 Randa rockslide. *Int. J. Rock Mech. Min.* **2004**, *41*, 69–87. [CrossRef]
14. Stead, D.; Eberhardt, E.; Coggan, J.S. Developments in the characterization of complex rock slope deformation and failure using numerical modelling techniques. *Eng. Geol.* **2006**, *83*, 217–235. [CrossRef]
15. Davies, T.R.; McSaveney, M.J. The role of rock fragmentation in the motion of large landslides. *Eng. Geol.* **2009**, *109*, 67–79. [CrossRef]
16. Qin, S.; Jiao, J.J.; Wang, S.A. Cusp Catastrophe Model of Instability of Slip-buckling Slope. *Rock Mech. Rock Eng.* **2001**, *34*, 119–134. [CrossRef]
17. Blikra, L.H.; Longva, O.; Harbitz, C.; Løvholt, F. Quantification of rock avalanche and tsunami hazard in Storfjorden, western Norway. In *Landslide and Avalanches*; Sennest, K., Flaate, K., Larsen, J.O., Eds.; Taylor and Francis Group: London, UK, 2005; pp. 7–63.
18. Bornhold, B.D.; Thomson, R.E. Tsunami hazard assessment related to slope failures in coastal waters. In *Landslides-Types, Mechanisms and Modeling*; Clague, J.J., Stead, D., Eds.; Cambridge University Press: Cambridge, UK, 2012; pp. 108–120.
19. Della Seta, M.; Martino, S.; Scarascia Mugnozza, G. Quaternary sea-level change and slope instability in coastal areas: Insights from the Vasto Landslide (Adriatic coast, central Italy). *Geomorphology* **2013**, *201*, 468–478. [CrossRef]
20. Chang, K.T.; Ge, L.; Lin, H.H. Slope creep behavior: Observations and simulations. *Environ. Earth Sci.* **2015**, *73*, 275–287. [CrossRef]

21. Piacentini, D.; Devoto, S.; Mantovani, M.; Pasuto, A.; Prampolini, M.; Soldati, M. Landslide susceptibility modelling assisted by Persistent Scatterers Interferometry (PSI): An example from the northwestern coast of Malta. *Nat. Hazards* **2015**, *78*, 681–697. [CrossRef]
22. Mantovani, M.; Devoto, S.; Piacentini, D.; Prampolini, M.; Soldati, M.; Pasuto, A. Advanced SAR interferometric analysis to support geomorphological interpretation of slow-moving coastal landslide (Malta, Mediterranean Sea). *Remote Sens.* **2016**, *8*, 443. [CrossRef]
23. Bezerra, F.H.R.; Barreto, A.M.F.; Suguio, K. Holocene sea-level history on the Rio Grande do Norte State coast, Brazil. *Mar. Geol.* **2003**, *196*, 73–89. [CrossRef]
24. Pellicani, R.; Miccoli, D.; Spilotro, G.; Gallipoli, M.R.; Mucciarelli, M.; Bianca, M. Dynamic response of a rocky cliff under the sea wave pulse: A study along the Adriatic coast of Polignano (Apulia, Italy). *Environ. Earth Sci.* **2015**, *73*, 6243–6257. [CrossRef]
25. Lambeck, K.; Antonioli, F.; Purcell, A.; Silenzi, S. Sea level change along the Italian coast for the past 10,000 yrs. *Quat. Sci. Rev.* **2004**, *23*, 1567–1598. [CrossRef]
26. Furlani, S. Integrating observational targets and instrumental data on rock coasts through snorkel surveys: A methodological approach. *Mar. Geol.* **2020**, *425*. [CrossRef]
27. Furlani, S.; Piacentini, D.; Troiani, F.; Biolchi, S.; Roccheggiani, M.; Tamburini, A.; Tirincanti, E.; Vaccher, V.; Antonioli, F.; Devoto, S.; et al. Tidal notches (Tn) along the western Adriatic coast as markers of local coastal stability during late Holocene. *Geogr. Fis. Din. Quat.* **2018**, *41*, 33–46.
28. Aringoli, D.; Gentili, B.; Materazzi, M.; Pambianchi, G.; Farabollini, P. Il ruolo della gravità nell'evoluzione geomorfologica di un'area di falesia: Il caso del Monte Conero (mare Adriatico, Italia Centrale). *Studi Costieri* **2014**, *22*, 19–32.
29. Montanari, A.; Mainiero, M.; Coccioni, R.; Pignocchi, G. Catastrophic landslide of medieval Portonovo (Ancona, Italy). *Geol. Soc. Am. Bull.* **2016**, *128*, 1660–1678. [CrossRef]
30. Mastronuzzi, G.; Aringoli, D.; Aucelli, P.; Baldassarre, M.A.; Bellotti, P.; Bini, M.; Biolchi, S.; Bontempi, S.; Brandolini, P.; Chelli, A.; et al. The geomorphological map of the Italian coast: From a descriptive to a morphodynamic approach. *Geogr. Fis. Din. Quat.* **2017**, *40*, 161–196.
31. Campobasso, C.; Carton, A.; Chelli, A.; D'Orefice, M.; Dramis, F.; Graciotti, R.; Guida, D.; Pambianchi, G.; Peduto, F.; Pellegrini, L. *Aggiornamento ed Integrazioni Delle Linee Guida Della Carta Geomorfologica d'Italia Alla Scala 1:50.000*; Quaderni serie III; ISPRA, Servizio Geologico d'Italia: Roma, Italy, 2018; Volume 13.
32. Florinsky, I.V. An illustrated introduction to general geomorphometry. *Progr. Phys. Geogr.* **2017**, *41*, 723–752. [CrossRef]
33. Hengel, T.; Reuter, H.I. *Geomorphometry: Concepts, Software, Applications*; Elsevier: Amsterdam, The Netherlands, 2009.
34. Burrough, P.A.; McDonell, R.A. *Principles of Geographical Information Systems*; Oxford University Press: New York, NY, USA, 1998.
35. McKean, J.; Roering, J. Objective landslide detection and surface morphology mapping using high-resolution airborne laser altimetry. *Geomorphology* **2004**, *57*, 331–351. [CrossRef]
36. Berti, M.; Corsini, A.; Daehne, A. Comparative analysis of surface roughness algorithms for the identification of active landslides. *Geomorphology* **2012**, *182*, 1–18. [CrossRef]
37. Hobson, R.D. Surface roughness in topography: Quantitative approach. In *Spatial Analysis in Geomorphology*; Chorley, R.J., Ed.; Harper & Row: New York, NY, USA, 1972; pp. 221–245.
38. Shepard, M.K.; Campbell, B.A.; Bulmer, M.H.; Farr, T.G.; Gaddis, L.R.; Plaut, J.J. The roughness of natural terrain: A planetary and remote sensing perspective. *J. Geophys. Res.* **2001**, *106*, 777–795. [CrossRef]
39. Guth, P.L. Terrain organization calculated from digital elevation models. In *Concepts and Modelling in Geomorphology: International Perspectives*; Evans, I.S., Dikau, R., Tokunaga, E., Ohmori, H., Hirano, M., Eds.; Terrapub: Tokyo, Japan, 2003; pp. 199–220.
40. Savelli, D.; Troiani, F.; Cavitolo, P.; Nesci, O. Rocky cliffs joining velvet beaches: The northern Marche coast. In *Landscapes and Landforms of Italy*; Marchetti, M., Soldati, M., Eds.; World Geomorphological Landscapes, Springer International Publishing AG: Cham, Switzerland, 2017; pp. 271–280.
41. Cello, G.; Coppola, L. Assetto geologico-strutturale dell'area anconetana e sua evoluzione Plio-Quaternaria. *Boll. Soc. Geol. Ital.* **1984**, *103*, 97–109.
42. Coltorti, M.; Nanni, T.; Rainone, M.L. Il contributo delle scienze della terra nell'elaborazione di un piano paesistico: L'esempio del Monte Conero (Marche). *Mem. Soc. Geol. Ital.* **1987**, *37*, 629–647.

43. Mortimore, R.N.; Lawrence, J.; Pope, D.; Duperret, A.; Genter, A. Coastal cliff geo hazards in weak rock: The UK chalk cliffs of Sussex. In *Coastal Chalk Cliff Instability*; Mortimore, R.N., Duperret, A., Eds.; Engineering Geology Special Publ. 20/1; Geological Society: London, UK, 2004; pp. 3–31.
44. Hungr, O.; Leroueil, S.; Picarelli, L. The Varnes classification of landslide types, an update. *Landslides* **2013**, *11*, 167–194. [CrossRef]
45. Coltorti, M.; Dramis, F. The chronology of Upper Pleistocene stratified slope-waste deposits in central Italy. *Permafr. Periglac.* **1995**, *6*, 235–242. [CrossRef]
46. Van Steijn, H. Stratified slope deposits: Periglacial and other processes involved. In *Ice-Marginal and Periglacial Processes and Sediments*; Martini, I.P., French, H.M., Perez Alberti, A., Eds.; Special Publications 354; Geological Society: London, UK, 2011; pp. 213–226.
47. Nesci, O.; Savelli, D. Cicli continentali tardo-quaternari lungo i tratti vallivi mediani delle Marche settentrionali. *Geogr. Fis. Din. Quat.* **1986**, *9*, 192–211.
48. Savelli, D.; Troiani, F.; Bruciapaglia, E.; Calderoni, G.; Cavitolo, P.; Dignani, A.; Ortu, E.; Teodori, S.; Veneri, F.; Nesci, O. The landslide-dammed paleolake of Montelago (North Marche Apennines, Italy): Geomorphological evolution and paleoenvironmental outlines. *Geogr. Fis. Din. Quat.* **2013**, *36*, 267–287.
49. Di Luzio, E.; Saroli, M.; Esposito, C.; Bianchi Fasani, G.; Cavinato, G.P.; Scarascia Mugnozza, G. Influence of structural framework on mountain slope deformation in the Maiella anticline (Central Apennines, Italy). *Geomorphology* **2004**, *60*, 417–432. [CrossRef]
50. Alfaro, P.; Delgado, J.; Esposito, C.; Tortosa, F.G.; Marmoni, G.M.; Martino, S. Time-dependent modelling of a mountain front retreat due to a fold-to-fault controlled lateral spreading. *Tectonophysics* **2019**, *773*, 228–233. [CrossRef]
51. McAffee, R.P.; Cruden, D.M. Landslides at Rock Glacier Site, Highwood Pass, Alberta. *Can. Geotech. J.* **1996**, *33*, 685–695. [CrossRef]
52. Nichol, S.L.; Hungr, O.; Evans, S.G. Large scale brittle and ductile toppling of rock slopes. *Can. Geotech. J.* **2002**, *39*, 773–788. [CrossRef]
53. Scarascia Mugnozza, G.; Bianchi Fasani, G.; Esposito, C.; Martino, S.; Saroli, M.; Di Luzio, E.; Evans, S.G. Rock avalanche and mountain slope deformation in a convex, dip-slope: The case of the Majella Massif (Central Italy). In *Landslide from Massive Rock Slope Failure*; Evans, S.G., Scarascia Mugnozza, G., Strom, A., Hermanns, R.L., Eds.; NATO Science Series 49; Springer: Dordrecht, The Netherlands, 2006.
54. Bloom, A.L. Teaching about relict, no-analog landscapes. *Geomorphology* **2002**, *47*, 303–311. [CrossRef]
55. Martino, S.; Prestininzi, A.; Romeo, R.W. Earthquake-induced ground failures in Italy from a reviewed database. *Nat. Hazards Earth Syst. Sci.* **2014**, *14*, 799–814. [CrossRef]